BACKGROUND-ERROR STATISTICS MODELLING IN A 3D VARIATIONAL DATA ASSIMILATION SCHEME: ESTIMATION AND IMPACT ON THE ANALYSES

Pierre Gauthier, Mark Buehner and Luc Fillion
Atmospheric Environment Service,
2121 Trans-Canada Hwy (#502)
Dorval, Québec, CANADA H9P 1J3

ABSTRACT

In its first implementation, the 3D variational (3D-var) assimilation system of the Canadian Atmospheric Environment Service (AES) was configured to be as close as possible to the previous statistical interpolation (SI) analysis. In particular, the analysis increments are constructed at a lower horizontal resolution on prescribed pressure levels and subsequently interpolated vertically to the η levels of the model. In the next version of the 3D-var, the analysis increments will be expressed in terms of the model's own vertical coordinate. This version also includes a new covariance model for the background-error in which the variances fully vary in physical space while the correlations are considered to be homogeneous, isotropic but non-separable. Following Bouttier *et al.* (1997), the multivariate formulation is introduced implicitly through changes of variables, some of which being empirically determined. The estimation of the background-error statistics is based on a time-series of differences between two short-term forecasts (the "NMC" method). The results are compared to estimates based on innovations. The impact of the new statistics on the analysis is shown through the analysis increments obtained in response to single observations of different types.

1. INTRODUCTION

Since June 1997, the Canadian Atmospheric Environment Service (AES) has replaced its previous statistical interpolation (SI) scheme with a 3D variational data assimilation (3D-var) for its global analysis (Gauthier *et al.*, 1998). The regional analysis is also done operationally with the 3D-var since September 1997 (Laroche *et al.*, 1998). In its first implementation, the 3D-var was configured to be as close as possible to the previous SI analysis which has permitted an evaluation of the impact of data selection on both the analysis and the resulting forecasts. In this formulation, the analysis increments for winds, geopotential and dew-point depression are produced on a prescribed set of pressure levels. In the final step of the analysis, these increments are interpolated vertically to the levels of the model and the hydrostatic relationship is used to derive analysis increments for temperature and surface pressure from those of the geopotential. This leads to many problems that can be avoided by doing the analysis directly on the model's own vertical levels in terms of temperature and specific humidity. This will be the formulation used in the next version of the 3D-var of AES which will also include a new covariance model for the background-error. The main focus of this paper is on the multivariate representation of background-error covariances and their estimation. A methodology based on lagged forecasts (Hoffman and Kalnay, 1983; Parrish and Derber,1992; Rabier *et al.*,1998; Bouttier *et al.*, 1997) from January 1997 was employed to estimate the covariances.

The covariance model is described in section 2. Due to the existing hydrostatic and geostrophic balance between temperature and winds, one has to consider cross-covariance terms between error made on winds and temperature. These are dealt with by introducing appropriate changes of variables, some of which are determined empirically by using linear regression to establish the nature of the relationship between winds and the hydrostatically and geostrophically balanced components of temperature and surface pressure. Section 3 introduces two methods to estimate background-error statistics: one based on lagged forecasts and another based on *innovations,* that is differences between observations and forecasts. The results are presented in section 4 and

the impact on the analyses is studied in section 5 by presenting analysis increments obtained in response to single observations of different types. We conclude in section 6 by indicating possible extensions of this work.

2. MULTIVARIATE RELATIONSHIPS AND THE BACKGROUND-ERROR COVARIANCE MODEL

The numerical weather prediction (NWP) model of the Canadian Meteorological Center (CMC) uses a terrain-following vertical coordinate

$$\eta = (p - p_T)/(p_s - p_T)$$

where p_T = 10 hPa is the pressure at the top of the model's domain. Its 28 levels are shown on Fig. 1 and a detailed description is given in Côté *et al.* (1998).

The model state can be defined as $\mathbf{X}= (u, v, T, ln\ q, ln\ p_S)^T$ where u and v are respectively the east-west (zonal) and north-south (meridional) wind components; T is temperature, q is specific humidity and p_s, surface pressure. Alternatively, the wind components can be represented in terms of the streamfunction Ψ and velocity potential χ which represents the rotational and divergent components of the wind field. This is convenient because distinct physical and dynamical processes govern these two components. We will therefore represent, the model state as

$$\mathbf{X}= (\Psi, \chi, T, ln\ q, ln\ p_S)^T \ .$$

In its discretized form, each of these variable is itself represented by a state vector of dimension of the order of 10^6.

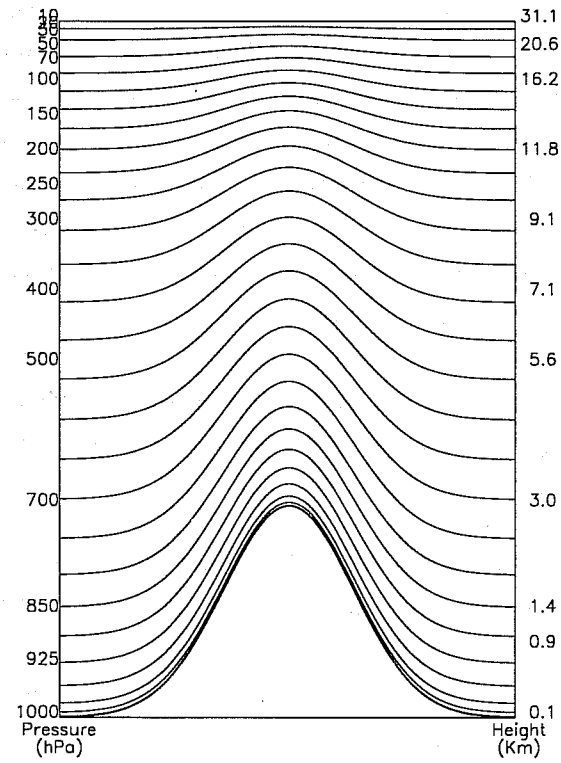

Fig.1: Vertical distribution of the 28 η levels of the CMC numerical weather prediction model.

A 3D scheme, by opposition to a 4D data assimilation scheme, takes the background-error statistics to be stationary in time. With the definition of model state given above, the background-error covariances describing the 6-h forecast error statistics can be expressed as

$$\mathbf{B}_\chi = \begin{pmatrix} \langle \Psi\Psi^T \rangle & \langle \Psi\chi^T \rangle & \langle \Psi T^T \rangle & \langle \Psi\, ln\, q^T \rangle & \langle \Psi\, ln\, p_s^T \rangle \\ \langle \chi\Psi^T \rangle & \langle \chi\chi^T \rangle & \langle \chi T^T \rangle & \langle \chi\, ln\, q^T \rangle & \langle \chi\, ln\, p_s^T \rangle \\ \langle T\Psi^T \rangle & \langle T\chi^T \rangle & \langle TT^T \rangle & \langle T\, ln\, q^T \rangle & \langle T\, ln\, p_s^T \rangle \\ \langle ln\, q\Psi^T \rangle & \langle ln\, q\chi^T \rangle & \langle ln\, qT^T \rangle & \langle ln\, q\, ln\, q^T \rangle & \langle ln\, q\, ln\, p_s^T \rangle \\ \langle ln\, p_s \Psi^T \rangle & \langle ln\, p_s \chi^T \rangle & \langle ln\, p_s T^T \rangle & \langle ln\, p_s\, ln\, q^T \rangle & \langle ln\, p_s\, ln\, p_s^T \rangle \end{pmatrix}, \tag{2.1}$$

where the brackets stand for a time average over a period of one to three months typically.

The underlying dynamics create a coupling between the error of these variables. For instance, mass and the streamfunction are coupled through the linear balance relationship

$$\nabla^2 P_B = \nabla \cdot f \nabla \Psi \Rightarrow P_B = \mathcal{B}(\varphi)\, \Psi \tag{2.2}$$

where $f = 2\Omega\, sin\, \varphi$ with φ, the latitude, and $\Omega = 2\pi/\tau$, is the angular frequency of the Earth with τ = 24h. In (2.2), the convention adopted is that $\mathcal{B}$ is a matrix relating the discretized state vector of Ψ to that of P_B. With the vertical discretization given above, the mass variable can be written as

$$P = \Phi + R\bar{T}\, ln\, p_s$$

with $\bar{T}$ = 300K being a constant reference temperature. The geopotential Φ is related to temperature through the hydrostatic relationship

$$\frac{\partial}{\partial \eta}\Phi(\eta) = R\, \frac{(p_s - p_T)}{\left(p_T(1-\eta) + \eta\, p_s\right)}\, T(\eta)\ , \tag{2.3}$$

where R = 287 J kg^{-1} K^{-1} is the gas constant for dry air. In its discretized form, (2.3) can be represented as T = A Φ and A is assumed independent of longitude or latitude, thereby neglecting the weak dependency of (2.3) on variations of surface pressure. Combining this with (2.2), the geostrophically balanced component of temperature T_B and surface pressure are

$$T_B = A\, \mathcal{B}\, \Psi = \mathcal{T}\, \Psi\ ,$$

$$(ln\, p_s)_B = (P_B/R\bar{T})\big|_{\eta=1} = \mathcal{S}\, \Psi\ .$$

The balanced component only represents part of both T and p_s and we introduce the unbalanced components of T and p_s as $T' = T - T_B$ and $(ln\, p_s') = ln\, p_s - (ln\, p_s)_B$ to represent the remaining component.

Another relationship exists between the streamfunction and the velocity potential through a typical Ekman balance relationship that causes winds to deviate from the geostrophic balance due to the presence of surface friction. This creates an inflow (outflow) towards the center of a low (high) pressure system. As noted in Polavarapu (1995), this establishes a partial coupling between the divergent wind component and the streamfunction which is mostly active near the surface of the model. As we did for temperature, we express the velocity potential as $\chi = \chi_B + \chi'$ and we assume an as yet undefined scalar relationship between χ_B and Ψ of the form $\chi_B(\lambda,\varphi,\eta) = E(\varphi,\eta)\, \Psi(\lambda,\varphi,\eta)$. This form is suggested by the Ekman layer dynamics that would make the coupling between Ψ and χ to depend on both latitude and altitude.

By introducing the change of variables

$$\mathbf{X} = \begin{bmatrix} \Psi \\ \chi \\ T \\ ln\, q \\ ln\, p_s \end{bmatrix} = \begin{pmatrix} \mathbf{I} & 0 & 0 & 0 & 0 \\ E & \mathbf{I} & 0 & 0 & 0 \\ \mathcal{T} & 0 & \mathbf{I} & 0 & 0 \\ 0 & 0 & 0 & \mathbf{I} & 0 \\ \mathcal{S} & 0 & 0 & 0 & \mathbf{I} \end{pmatrix} \begin{bmatrix} \Psi \\ \chi' \\ T' \\ ln\, q \\ ln\, p_s' \end{bmatrix} \equiv \mathcal{M} \begin{bmatrix} \Psi \\ \chi' \\ T' \\ ln\, q \\ ln\, p_s' \end{bmatrix} \equiv \mathcal{M}\, \mathbf{X}' \,, \tag{2.4}$$

we assume that the dependencies between the analysis variables are eliminated. Therefore, in terms of these variables, the error covariance model $\mathbf{B}_{X'}$ is

$$\mathbf{B}_{X'} = \begin{pmatrix} \langle \Psi\Psi^T \rangle & 0 & 0 & 0 & 0 \\ 0 & \langle \chi'\chi'^T \rangle & 0 & 0 & 0 \\ 0 & 0 & \langle T'T'^T \rangle & 0 & 0 \\ 0 & 0 & 0 & \langle ln\, q\, ln\, q^T \rangle & 0 \\ 0 & 0 & 0 & 0 & \langle ln\, p_s'\, ln\, p_s'^T \rangle \end{pmatrix}. \tag{2.5}$$

The covariances $\mathbf{B}_X$ are implicitly defined from (2.4) and (2.5) and are

$$\mathbf{B}_X = \mathcal{M}\, \mathbf{B}_{X'}\, \mathcal{M}^T$$

$$= \begin{pmatrix} \mathbf{B}_{\Psi\Psi} & \mathbf{B}_{\Psi\Psi}E^T & \mathbf{B}_{\Psi\Psi}\mathcal{T}^T & 0 & \mathbf{B}_{\Psi\Psi}\mathcal{S}^T \\ E\mathbf{B}_{\Psi\Psi} & \left[\mathbf{B}_{\chi'\chi'} + E\mathbf{B}_{\Psi\Psi}E^T\right] & E\mathbf{B}_{\Psi\Psi}\mathcal{T}^T & 0 & E\mathbf{B}_{\Psi\Psi}\mathcal{S}^T \\ \mathcal{T}\mathbf{B}_{\Psi\Psi} & \mathcal{T}\mathbf{B}_{\Psi\Psi}E^T & \left[\mathcal{T}\mathbf{B}_{\Psi\Psi}\mathcal{T}^T + \mathbf{B}_{TT'}\right] & 0 & \mathcal{T}\mathbf{B}_{\Psi\Psi}\mathcal{S}^T \\ 0 & 0 & 0 & \mathbf{B}_{ln q\, ln q} & 0 \\ \mathcal{S}\mathbf{B}_{\Psi\Psi} & \mathcal{S}\,\mathbf{B}_{\Psi\Psi}E^T & \mathcal{S}\mathbf{B}_{\Psi\Psi}\mathcal{T}^T & 0 & \left[\mathcal{S}\,\mathbf{B}_{\Psi\Psi}\mathcal{S}^T + \mathbf{B}_{ln p_s'\, ln p_s'}\right] \end{pmatrix}. \tag{2.6}$$

The only cross-terms appearing in (2.6) are due to the geostrophic and Ekman coupling involving the streamfunction.

The covariances can be factorized as

$$\mathbf{B}_{X'} = \mathbf{D}\,\mathbf{C}\,\mathbf{D}$$

where the diagonal matrix $\mathbf{D}$

$$\mathbf{D} = \begin{pmatrix} \sigma_\Psi & 0 & 0 & 0 & 0 \\ 0 & \sigma_\chi & 0 & 0 & 0 \\ 0 & 0 & \sigma_{T'} & 0 & 0 \\ 0 & 0 & 0 & \sigma_{lnq} & 0 \\ 0 & 0 & 0 & 0 & \sigma_{lnp_s'} \end{pmatrix}$$

and the block-diagonal matrix $\mathbf{C}$

$$\mathbf{C} = \begin{pmatrix} \mathbf{C}_{\Psi\Psi} & 0 & 0 & 0 & 0 \\ 0 & \mathbf{C}_{\chi'\chi'} & 0 & 0 & 0 \\ 0 & 0 & \mathbf{C}_{T'T'} & 0 & 0 \\ 0 & 0 & 0 & \mathbf{C}_{lnq\, lnq} & 0 \\ 0 & 0 & 0 & 0 & \mathbf{C}_{lnp_s'\, lnp_s'} \end{pmatrix}$$

stand respectively for the standard deviations (which vary with latitude and level) and correlations of the analysis variables.

The background-error correlations for all analysis variables are taken to be horizontally homogeneous and isotropic which means that

$$\langle \varepsilon(p,\eta_p)\, \varepsilon(q,\eta_q) \rangle = F(r,\eta_p,\eta_q)$$

with ε being the normalized background-error for any of the analysis variables. The correlations therefore only depend on the horizontal distance r between the two points p and q. In spherical coordinates having their pole set at p where $r = 0$, the correlation function F can be expanded in a series of zonal spherical harmonics as

$$F(r, \eta_p, \eta_q) = \sum_{n=0}^{N} \tilde{a}_n(\eta_p, \eta_q)\, Y_{Pn}^{0}(\mu), \qquad (2.7)$$

where $r = a \cos^{-1}\mu$ is the great circle distance from the pole, a is the radius of the Earth and $Y_{Pn}^{0}(\mu)$ stands for the zonal spherical harmonics (the subscript p stresses that these coordinates have their pole at point p). Referring to Boer (1983), Gauthier *et al.* (1993) and Courtier *et al.* (1998), one can use the addition theorem for spherical harmonics to show that the correlation between two spectral components (m,n,η_p),and (m',n',η_q) is

$$\begin{aligned} \tilde{C}_{n,n'}^{m,m'} &= \langle \tilde{\varepsilon}_n^{m}(\eta_p)\, \tilde{\varepsilon}_{n'}^{-m'}(\eta_q) \rangle \\ &= \tilde{a}_n(\eta_p,\eta_q)\, \left(\sqrt{2n+1}\right)^{-1} \delta_{n=n'}\, \delta_{m=-m'} \end{aligned}$$

and $\tilde{\mathbf{C}}$ is therefore block-diagonal, the entries of which do not depend on the zonal wavenumber m. This leads to a compact representation of the correlations that can be expressed as

$$\mathbf{C} = \mathbf{S}^{-1}\, \tilde{\mathbf{C}}\, (\mathbf{S}^{-1})^{T}$$

where $\mathbf{S}^{-1}$ is the inverse spectral transform.

In summary, the covariance model used here is univariate in terms of the analysis variables $\mathbf{X}'$. The correlations are assumed to be horizontally homogeneous, isotropic and non-separable while the standard deviations are allowed to vary as a function of latitude and vertical level. In the 3D-var, error covariances for the model's variables $\mathbf{X}$ are only implicitly defined through change of variables. For instance, it has been shown that the temperature error covariances are

$$\langle \underline{T}\underline{T}^{T} \rangle = \langle \underline{T}_B \underline{T}_B^{T} \rangle + \langle \underline{T}'\underline{T}'^{T} \rangle = \left[\mathcal{T}\, \mathbf{B}_{\Psi\Psi}\, \mathcal{T}^{T} + \mathbf{B}_{TT'} \right] .$$

Part of the error is then related to the wind error (through $\mathbf{B}_{\Psi\Psi}$).

3. ESTIMATION OF THE BACKGROUND-ERROR COVARIANCES

To estimate the background-error covariances for the model described in the previous section, two routes can be taken. One can compare the short-term forecasts against reliable and accurate observations, such as radiosonde data of geopotential, temperature, winds and humidity. Referring to Hollingsworth and Lönnberg (1986) and Mitchell *et al.* (1990), the observational error can be assumed to be uncorrelated between radiosondes and this permits to obtain estimates of parameters describing the horizontal correlations of the background-error for Ψ, for instance. Estimates of the background-error variance can be obtained as well but care must be taken to take into account that the observations are not without error themselves. The main difficulty with this approach is that the data coverage is rather sparse over large portions of the globe such as the oceans and the Southern Hemisphere. Even over a data dense region like North America, reliable estimates can only be obtained by collecting data over a period of two to three months. In the end, estimates of the characteristic length of correlation functions are obtained. The estimate of the variances are representative of their average over a rather

large latitudinal band. A statistical study of the innovation values $\upsilon = (\mathbf{y} - \boldsymbol{H}\boldsymbol{x}_b)$ can be very revealing about the performance of the assimilation system as a whole (Daley, 1992; Dee, 1995).

The origin of forecast error is due to several factors. There is of course the fact that NWP models are far from perfect and that we are not modelling correctly several atmospheric processes. There is also the presence of dynamical instabilities in the atmospheric flow which vary in time and space. The forecast error covariances used in the 3D-var are stationary and representative of the forecast error averaged over a season typically. One way that has been found useful and practical to estimate the background-error covariances is to use a lagged forecast approach. Considering a suite of forecasts $\mathbf{X}_i^{(T)}$ valid at time t_i obtained from initial conditions valid at time $t = t_i - T$, the forecast error is equated to

$$\delta\mathbf{x}_i = \mathbf{X}_i^{(T_2)} - \mathbf{X}_i^{(T_1)}$$

with $\Delta T = T_2 - T_1$ being the lag between the two forecasts. Typically, Parrish and Derber (1992) and Rabier *et al.* (1998) have used $T_2 = 48$ hrs and $T_1 = 24$ hrs. By choosing $T_1 = 24$ hrs, the spin-up of the model due to initial imbalances is avoided and the forecast differences are then assumed to be more representative of the forecast error. Rabier *et al.* (1998) used different values for T_1 and ΔT and did not observe significant variations of their results. In our present study, a lag $\Delta T = 24$ hrs with $T_1 = 24$ hrs has been considered.

A schematic of the lagged forecasts method is shown in Fig. 2. Information from observations over a period ΔT will introduce a perturbation between the two states at $t = t_i + T$ representative of the initial error. This error then evolves dynamically according to the model's dynamics thereby introducing some error growth or damping depending on the local stability properties of the flow. Both of these hypotheses can be questioned. The representativeness of the initial perturbation is very much dependent on the observational network while the dynamics of error growth assumes that the model is in a sense perfect. In regions where there are no observations, the initial conditions are left unchanged so that the initial difference is virtually zero and integrating it over a period of time ΔT still leaves us with a vanishingly small quantity. This would lead us to the erroneous conclusion that there is no forecast error in regions where there are no observations. Moreover, if the model has excessive damping, it would reduce the initial difference in an unrealistic manner which would again bring us to

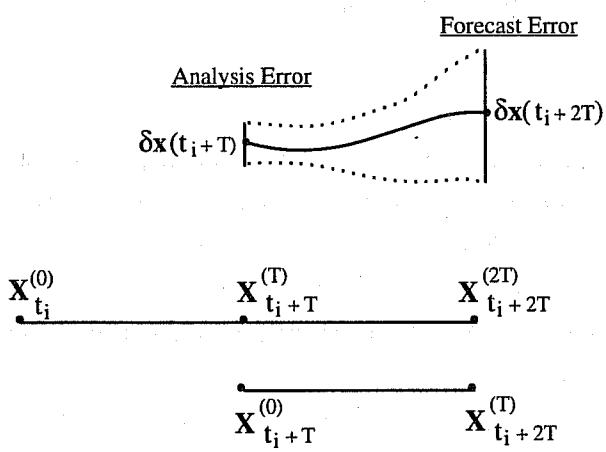

Fig. 2: Schematic of the lagged forecast scheme. The difference $\delta\mathbf{x}(t_i + T) = \mathbf{X}^{(T)}_{t_i+T} - \mathbf{X}^{(0)}_{t_i+T}$ corresponds to perturbations brought to the initial conditions by the observations contained in the time interval $[t_i, t_i + T]$. Local dynamical instabilities cause this initial perturbation to grow up to time $t_i + 2T$.

the wrong conclusion. Now that these possible limitations have been stated, we will nevertheless assume that the δx_k are indeed representative of forecast error, at least in terms of their averaged statistics. We now describe how the forecast error statistics are obtained.

Considering the ensemble average

$$\langle \delta x \rangle = \frac{1}{K} \sum_{k=1}^{K} \delta x_k \ , \tag{3.1}$$

the *unbiased increments* are $\delta x'_k = \delta x_k - \langle \delta x \rangle$ and the unbiased estimate of the variance is given by

$$\sigma^2 = \frac{1}{K\text{-}1} \sum_{k=1}^{K} \delta x'^2_k = \frac{1}{K\text{-}1} \sum_{k=1}^{K} \delta x_k^2 - \frac{K}{K\text{-}1} \langle \delta x \rangle^2 \ . \tag{3.2}$$

provided any two error vectors δx_i and δx_j are statistically independent.

The *normalized increments* are defined as

$$X'_k = \delta x'_k / \sigma \tag{3.3}$$

and are such that $\langle X' \rangle = 0$ and $\sigma^2_{X'} = 1$.

If these correlations are homogeneous and isotropic in the horizontal, it follows that

$$\left\langle \tilde{X}^m_n(\eta_p)\, \tilde{X}^{m'}_{n'}(\eta_q) \right\rangle = \tilde{C}_n(\eta_p,\eta_q)\, \delta_{n=n'}\, \delta_{m=-m'} \ ,$$

where $\tilde{X}^m_n(\eta_p) = \left(S^m_n X'_k \right)$. In reality, the correlations are not expected to meet this condition exactly so that we define

$$\tilde{C}_n(\eta_p,\eta_q) = \frac{1}{2N+1} \sum_{m=-n}^{+n} \left\langle \tilde{X}^m_n(\eta_p)\, \tilde{X}^{-m}_n(\eta_q) \right\rangle \ . \tag{3.4}$$

The coefficients characterizing the correlation function (2.7) are given by

$$\tilde{a}_n(\eta_p,\eta_q) = \tilde{C}_n(\eta_p,\eta_q)\ \sqrt{2n+1} \ . \tag{3.5}$$

In summary, the estimation of the correlation then consists of the following steps:

i. Compute the forecast differences $\delta x_i = X_i^{(T_2)} - X_i^{(T_1)}$, their bias estimate $\langle \delta x \rangle$ and their variance σ using (3.1) and (3.2);

ii. Build the normalized increments X'_k using (3.3);

iii. Compute the spectral coefficients for ψ, χ', T', *ln* q and $ln p'_s$ to obtain the coefficients of the correlation function from (3.4) and (3.5).

Before doing this, it is necessary to first establish the definition of the balanced components of temperature T_B and velocity potential χ_B. As mentioned in section 2, T_B is related to the streamfunction by $T_B = A\, \mathcal{B}\, \Psi$ where $\mathcal{B}$ stands for the linear balance (2.2). We follow Bouttier *et al.* (1997) and use linear regression to determine the vertical operator A by finding that A which minimizes the variance of T'. The analytical form is used for the linear balance operator itself. Similarly, the relationship between χ_B and Ψ is defined as

$$\chi_B(\lambda,\varphi,\eta) = E(\varphi,\eta)\, \Psi\, (\lambda,\varphi,\eta) \ . \tag{3.6}$$

In that case, E is obtained by minimizing the variance of χ'.

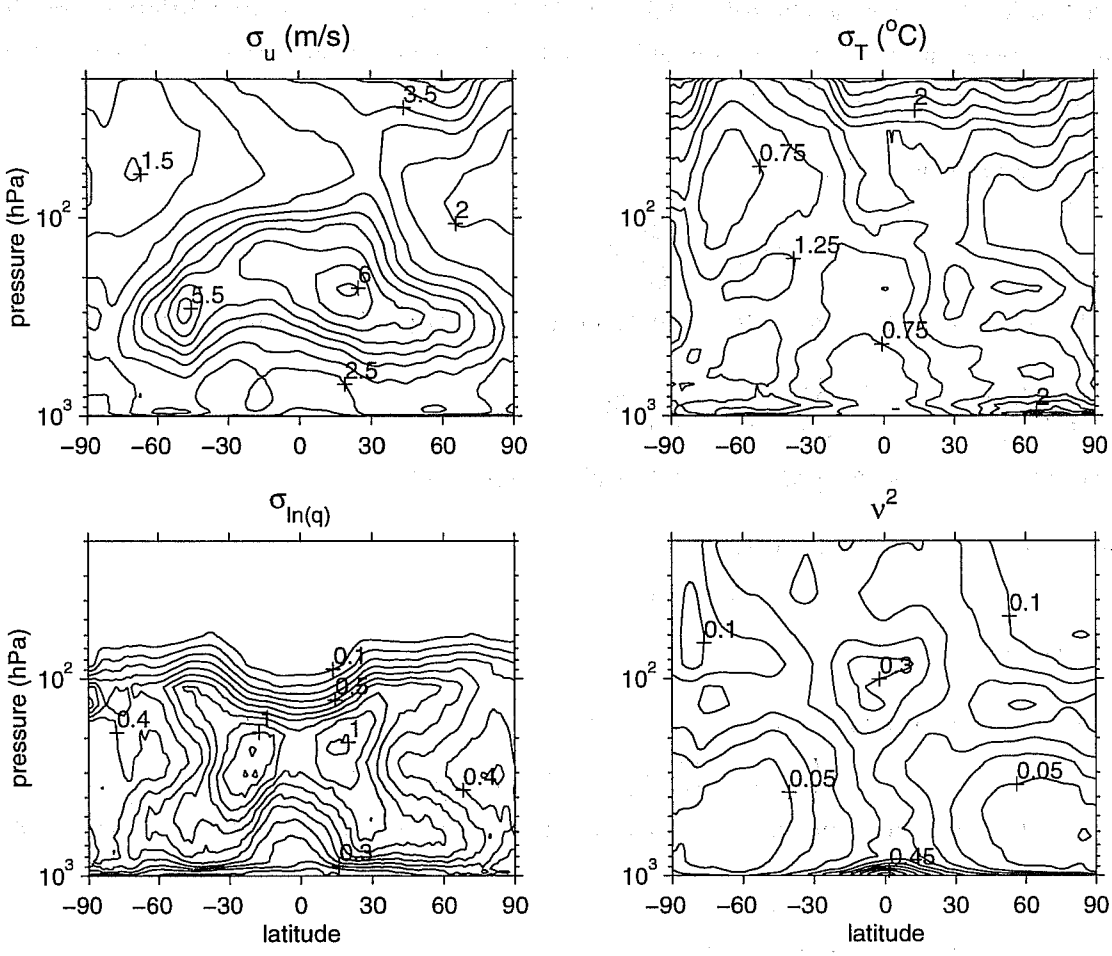

Fig. 3: Implicit variances for winds (σ_u^2), temperature (σ_T^2) and logarithm of specific humidity ($\sigma_{ln\,q}^2$) implied from the statistics of the analysis variables. Also shown is the ratio ν^2 of the divergent component of the kinetic energy of the wind error to the total kinetic energy.

4. RESULTS

The variances of the analysis variables Ψ, χ', T', *ln* p_s' and *ln* q implicitly define those of winds, temperature and the logarithm of specific humidity (*ln* q). These are shown in Fig. 3 which also shows the ratio $\nu^2(\varphi,\eta)$ of the divergent component of kinetic energy to the total kinetic energy of the wind error. The divergent component includes the balanced component χ_B and is active mostly in the tropics and near the surface.

Fig. 4 shows the ratio of $\sigma_{T'}^2$ to the total temperature variance, σ_T^2. The unbalanced component explains all the temperature variance in the tropics since the geostrophic balance does not apply. Fig.5 shows a similar ratio of $\sigma_{\chi'}^2$ to σ_χ^2 that is close to 1 in the tropics and at high altitudes where the divergent component is found to be uncorrelated from Ψ. The ratio is shown in Fig.5 only from the ground up to 700 hPa. This picture is consistent with the dynamics of Ekman dynamics which would be active near the surface but only in the extratropics.

Referring to Daley (1991), the characteristic length L is a measure of the local curvature of the horizontal correlations and is defined as

$$L^2(\eta) = -\frac{2\,F(0,\eta,\eta)}{\nabla^2 F(0,\eta,\eta)} \,. \qquad (4.1)$$

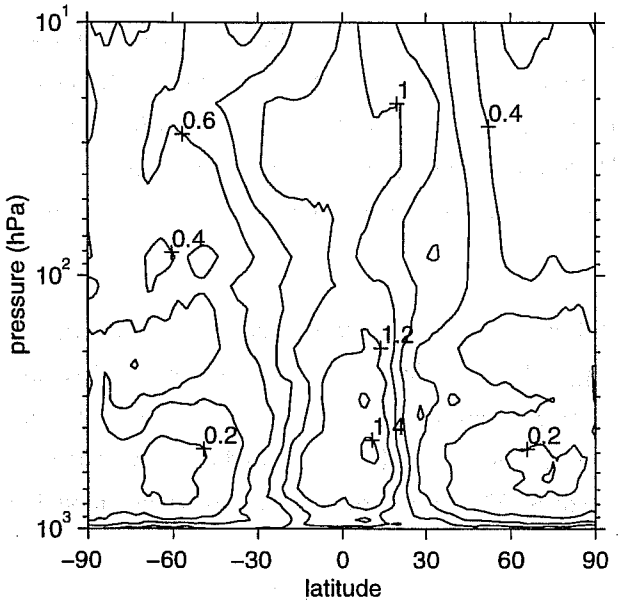

Fig.4: Ratio of variance of the unbalanced temperature $\sigma^2_{T'}$ to the total temperature variance σ^2_T as a function of height and latitude.

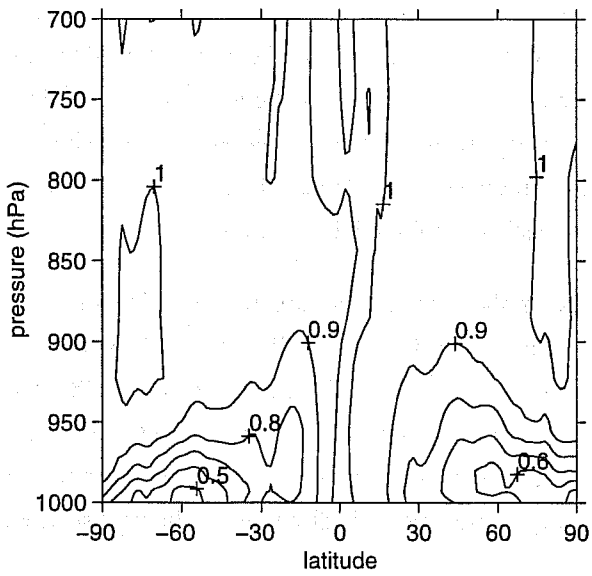

Fig.5: Ratio of variance of unbalanced velocity potential $\sigma^2_{\chi'}$ to the total variance σ^2_χ as a function of height and latitude.

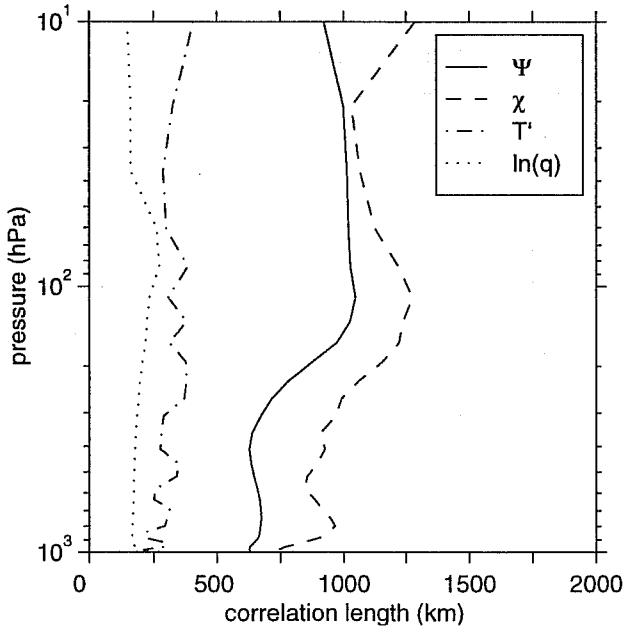

Fig. 6: Characteristic lengths of the horizontal correlations of Ψ, χ', T' and *ln* q as a function of height (in hPa).

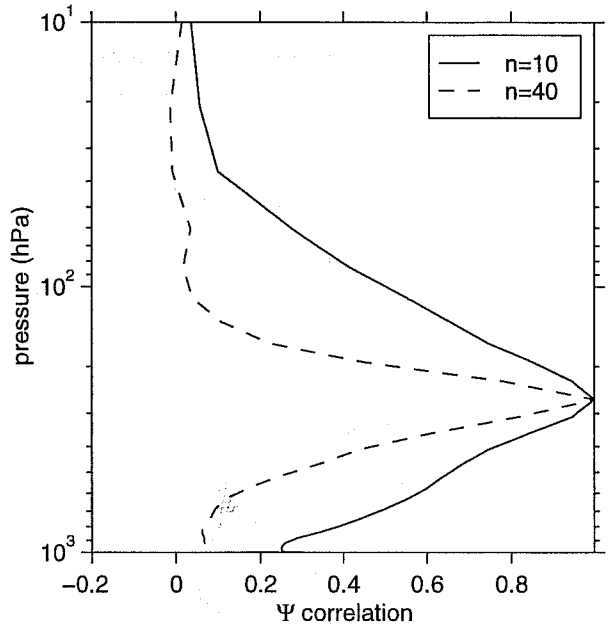

Fig. 7: Vertical correlations $\tilde{C}_n(\eta_p = 0.242, \eta_q)$ of the streamfunction Ψ for wavenumbers 10 and 40. This shows that the vertical correlations associated with shorter horizontal scales are sharper.

Those derived from the correlations of ψ, χ', T' and $ln\ q$ are shown in Fig.6 as a function of height. A noticeable feature is the increase in lengthscale at altitudes above the tropopause (~250 hPa). The oscillatory behavior of the lengthscale of T' could be traced back to the temperature forecast of the model itself. We came to this conclusion by computing the lengthscale associated with the departure of the 48-hrs forecast with respect to its monthly mean. A similar pattern to that shown in Fig.6 was obtained when using forecasts from this experimental version of the GEM model but not when this computation was based on forecasts from the operational spectral model operational.

The implied covariances are all derived from those of Ψ. Fig.7 shows the spectral coefficients $\tilde{a}_n(\eta_p,\eta_q)$ of the vertical correlations of Ψ for n = 10 and 40 when $\eta_p = 0.242$. They have been normalized so that $\tilde{a}_n(\eta_p,\eta_p) = 1$. As noted by Rabier *et al.* (1998), the vertical correlations are sharper for shorter horizontal scales. By differentiating Ψ to obtain winds, more emphasis is put on the smaller scales and the consequence is that derived correlations for winds will be sharper than those of Ψ. The impact of the new covariance model on the analysis increments is discussed in the next section.

As mentioned at the beginning of section3, the variances can also be estimated from innovations values obtained by comparing a 6-h forecast with radiosonde data. The variances estimated with this method are presented in Fig.8 for winds (solid line in left panel) and temperature (solid line in right panel): these were obtained by using all radiosonde data in the Northern Hemisphere (north of 20°) for January 1997 and the method used is described in Mitchell *et al.* (1990). These compare well with the corresponding estimates from

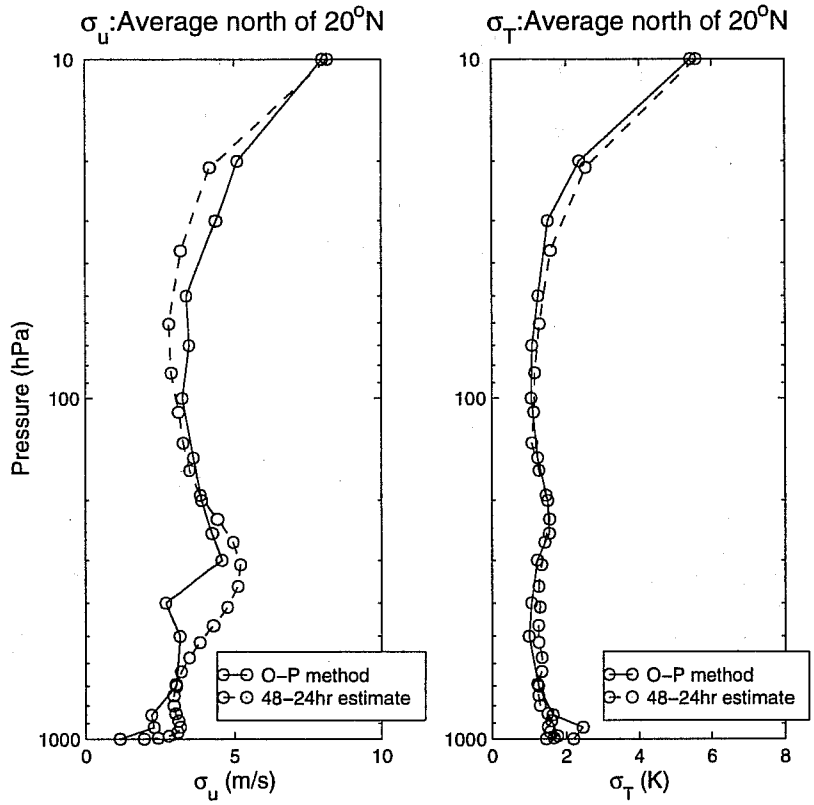

Fig. 8: Forecast error variances for winds (left panel) and temperature (right panel) estimated from the lagged forecasts (dashed line) and by a comparison to radiosonde data (solid line) over the Northern Hemisphere. The results of the lagged forecasts have been averaged over the Northern Hemisphere to make the results comparable.

the lagged forecasts averaged over the same area (shown as dashed lines in Fig.8) particularly for temperature. Some discrepancies between the two methods can be noted. For winds near 400 hPa, the comparison to radiosonde data suffers from a sampling error and shows a dependency on how the data are first binned and averaged before a fit is done. On the other hand, the variances of temperature are slightly underestimated near the surface by the lagged forecasts. These results give us some confidence in the background error variances estimates shown on Fig.3. Those were then used without modifications.

5. IMPACT ON THE ANALYSIS: SINGLE OBSERVATION EXPERIMENTS

Referring to (2.3) and (2.4), the analysis increment $\Delta\mathbf{X} = \mathbf{X}_a - \mathbf{X}_b$ is directly proportional to the covariances when a single observation of wind, temperature or specific humidity is assimilated. These *single observation* experiments are very useful to obtain a representation of the implicit covariances induced by the covariance model described above.

In Fig. 9, the solid curve shows the vertical profile of the zonal wind analysis increment obtained in response to a single observation of the zonal wind component at the level $\eta = 0.242$ (~ 250 hPa) at the latitude 45N (Sable Island). By comparison, the corresponding wind increment is represented when the current operational statistics are used (dashed curve). To facilitate the comparison, the two increments have been normalized to 1. The impact of the new statistics is to produce a sharper wind increment. This change in the vertical structure can be directly related to the non-separable correlation model used here. In the operational model, the vertical correlations used for winds correspond exactly to those of the stream function. To compare, the vertical error correlation of $C_\Psi(\eta_p = 0.242,\eta_q)$ has also been plotted in Fig.9 (dotted curve) and agrees well with the increment of the operational model. As discussed earlier, the fact that the new correlations are sharper at shorter horizontal scales leads to different vertical correlations for winds than those defined for Ψ. In the separable representation of Gauthier *et al.* (1998), the vertical correlations are the same at all wavenumbers.

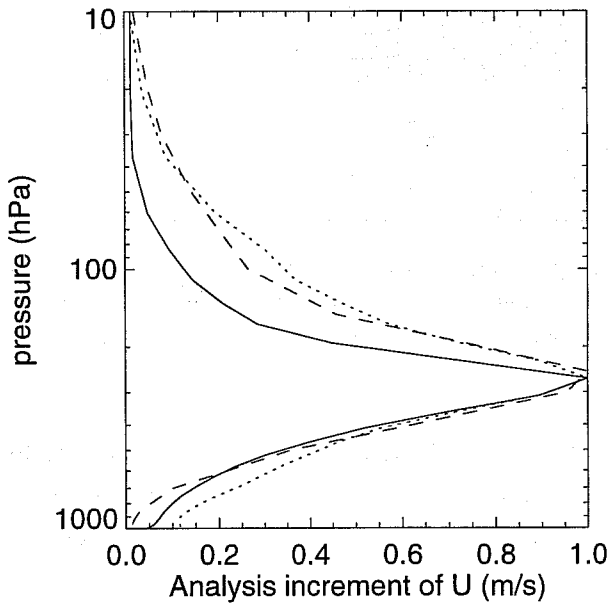

Fig. 9: Analysis increments obtained in response to a single observation of *u* located at the level 250 hPa for the new covariance model (solid line) and the covariance model used operationally (dashed line). The vertical correlation $C_\Psi(\eta_p = 0.242,\eta_q)$ has also been plotted. To permit the comparison, all three curves have been normalized.

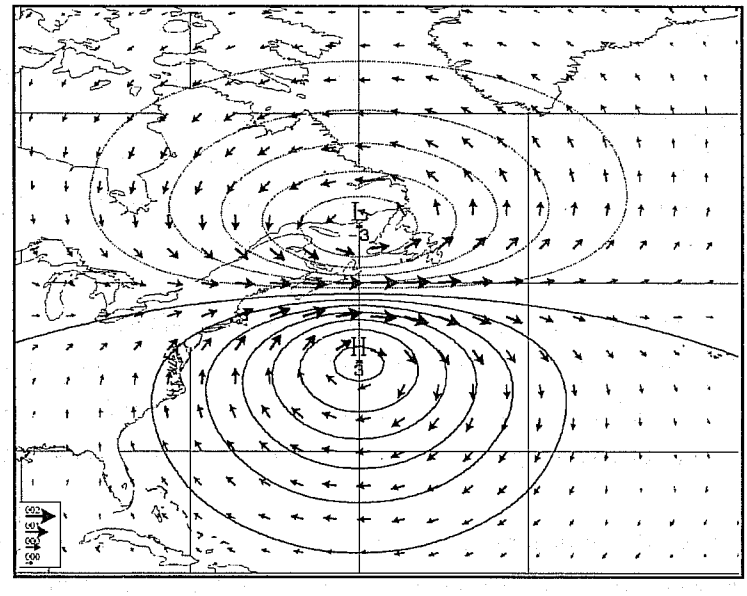

Fig. 10: Streamfunction and wind increments obtained in response to a single observation of zonal wind located at 265 hPa in the Northern extratropics (45N, 60W).

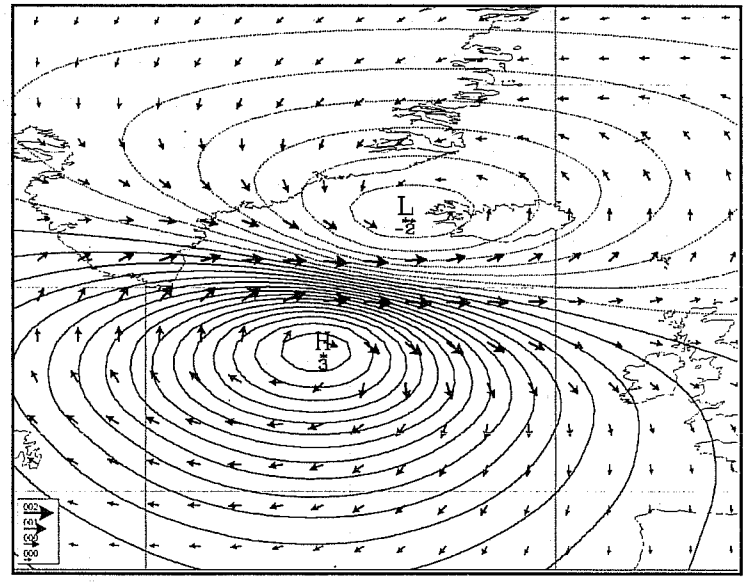

Fig. 11: As in Fig. 10 but when the wind observation is located at the surface and at (60N, 30W). The balanced component of the divergence is creating an inflow towards the center of the low pressure system (Ψ negative) and an outflow emerging from the center of the high pressure system (Ψ positive).

The horizontal structure of the analysis increment is shown in Fig.10 and the circulation is approximately geostrophic as expected. The cross-terms of the covariances (2.6) imply that this wind observation has an impact on temperature and divergence (not shown).Similarly, Fig. 11 shows the analysis wind increments in response to a single zonal wind observation located near the surface at 60N where the balanced component of the velocity potential is the most active. The winds are converging towards the inside (outside) of the low (high) pressure system as would be expected when surface friction is present.

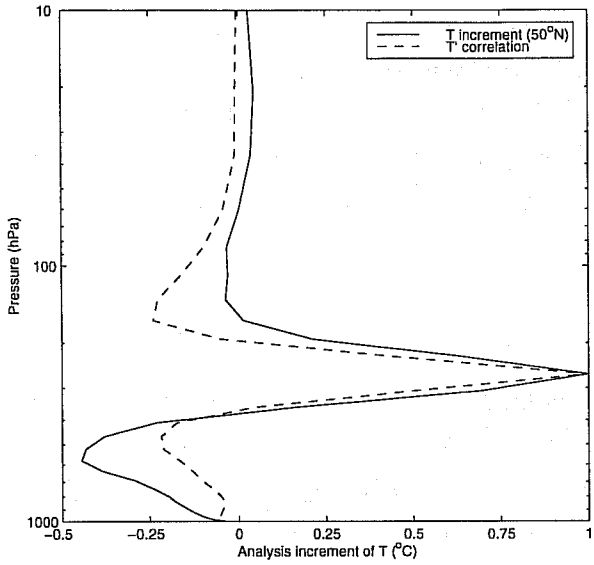

Fig. 12: Analysis increment for temperature (solid line) in response to a single observation of temperature located at 50N and 242 hPa. The vertical correlation of T' for this level has been superimposed. To permit comparison, the analysis increment has been normalized.

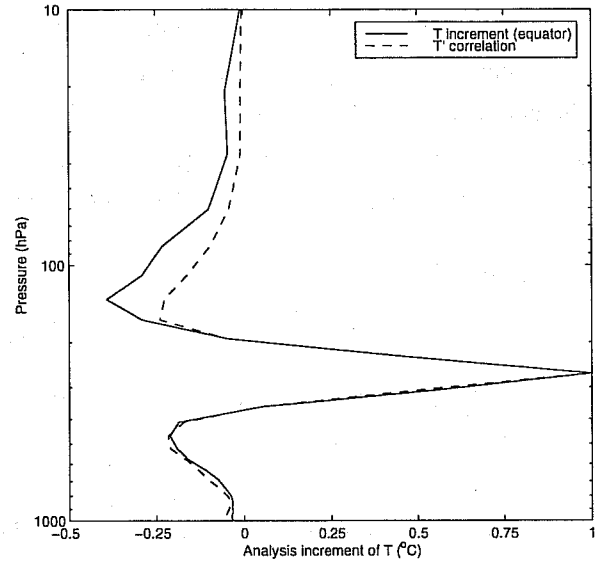

Fig. 13: As in Fig.13 but when the temperature observation is located at the equator.

Temperature normalized increments are shown in Fig.12 and 13 in response to a single observation located at 50N and the equator respectively. These are shown as solid lines and compared to the vertical correlations of T'. The broadening of the temperature increment in the extratropics can be attributed to the balanced component of temperature by the broader correlations used for Ψ. The difference between the correlation shown on Fig.13 and the normalized temperature increment is due to the vertical variation of the variances.

6. CONCLUSION

In this paper, the covariance model used in the new version of the 3D-var of AES has been described. It is similar in many ways to that introduced by Bouttier *et al.* (1997) and uses a non-separable correlation model that leads to sharper wind and temperature increments. Empirical relationships have been obtained to define the balanced components of temperature and divergence. The form used to obtain the balanced temperature was suggested by the analytical form of the hydrostatic relationship while the form used for the balanced component of divergence is defined in physical space and is a function of latitude and height. The motivation for the latter form came from the Ekman layer dynamics. This work is still ongoing and the next step is to conduct an extensive set of experiments to assess the impact of these changes on the forecasts. The nature of these experiments is similar to those described in Gauthier *et al.* (1998).

Because the background-error covariances play a key role in the analysis, the 3D-var system of AES has been designed to handle more complex representations of the background-error covariances than was possible in our previous statistical interpolation analysis. However, the removal of the assumption of stationarity of the background-error statistics can only be achieved by casting the problem in a quadri-dimensional context. Using a

simplified Kalman filter (Fisher and Courtier, 1995; Fisher, 1998) or an ensemble approach (Houtekamer and Mitchell, 1998), approximations to the background error can be obtained to bring more realism to the covariance model. Nothing precludes the introduction of such models in a 3D-var framework. The benefit would be to have analysis increments with flow dependent baroclinic structures (Thépaut *et al.*, 1995) capable of discriminating whether the development of a meteorological system should be triggered or not. This would be an intermediate level 4D data assimilation scheme that would improve upon the current formulation of the 3D-var.

7. REFERENCES

Boer, G.J., 1983: Homogeneous and isotropic turbulence on the sphere. *J. Atmos. Sci.*, **40**, 154-163.

Bouttier, F., J. Derber and M. Fisher, 1997: The 1997 revision of the Jb term in 3D/4D-Var. *ECMWF Research Dept.,* Technical Memorandum No.238, ECMWF, Reading, U.K., 53 pages.

Côté, J., S. Gravel, A. Méthot, A. Patoine, M. Roch and A.N. Staniforth, 1998: The operational CMC/MRB global environmental multiscale (GEM) model: Part I- Design considerations and formulation. *Mon. Wea. Rev.,* **120**, 1373-1395.

Courtier, P., E. Andersson, W. Heckley, J. Pailleux, D. Vasiljevic, M. Hamrud, A. Hollingsworth, F. Rabier and M. Fisher, 1998: The ECMWF implementation of three dimensional variational assimilation (3D-Var). Part I: formulation. *Quart. J.R. Meteor. Soc.*, **124**, 1783-1808.

Daley, R., 1992: The lagged innovation covariance: a performance diagnostic for atmospheric data assimilation. *Mon. Wea. Rev.*, **120**, 178-196.

Daley, R., 1991: *Atmospheric Data Analysis.* Cambridge University Press, Cambridge, 457 pages.

Dee, D.P., 1995: On-line estimation of error covariance parameters for atmospheric data assimilation. *Mon. Wea. Rev.,* **123**, 1128-1145.

Fisher, M., 1998: Development of a simplified Kalman filter. *ECMWF Technical Memo. No. 260,* Reading U.K., 16 pages.

Fisher, M. and P. Courtier, 1995: Estimating the covariance matrices of analysis and forecast error in variational data assimilation. *ECMWF Technical Memo. No. 220,* Reading U.K., 28 pages.

Gauthier, P., C. Charette, L. Fillion, P. Koclas and S. Laroche, 1998: Implementation of a 3D variational data assimilation system at the Canadian Meteorological Centre. Part I: The global analysis. (submitted to *Atmosphere-Ocean*).

Gauthier, P., P. Courtier and P. Moll, 1993: Assimilation of simulated wind Lidar data with a Kalman filter. *Mon. Wea. Rev.,* **121**, 1803-1820.

Hoffman, R.N. and E. Kalnay, 1983: Lagged average forecasting, an alternative to Monte Carlo forecasting. *Tellus,* **35A**, 100-118.

Hollingsworth, A. and P. Lönnberg, 1986: The statistical structure of short-range forecast errors as determined from radiosonde data. Part I: the wind field. *Tellus,* **38A**, 111-136.

Houtekamer, P. and H.L. Mitchell, 1998: Data assimilation using an ensemble Kalman filter technique. *Mon. Wea. Rev.*, **126**, 796-811.

Laroche, S., P. Gauthier, J. Saint-James and J. Morneau, 1998: Implementation of a 3D variational data assimilation system at the Canadian Meteorological Centre. Part II: The regional analysis. (submitted to *Atmosphere-Ocean*).

Mitchell, H.L., C. Charette, C. Chouinard, B. Brasnett, 1990: Revised interpolation statistics for the Canadian Data assimilation procedure: their derivation and application. *Mon. Wea. Rev.*, **118**, 1591-1614.

Parrish, D.F., and J.C. Derber, 1992: The National Meteorological Center's spectral statistical interpolation analysis system. *Mon. Wea. Rev.*, **120**, 1747-1763.

Polavarapu, S., 1995: Divergent wind analyses in the oceanic boundary layer. *Tellus,* **47A**, 221-239.

Rabier, F., J.F. Mahfouf, M. Fisher, H. Järvinen, A. Simmons, E. Andersson, F. Bouttier, P. Courtier, M. Hamrud, J. Haseler, A. Hollingsworth, L. Isaksen, E. Klinker, S. Saarinen, C. Temperton, J.N. Thépaut, P.Undén and D. Vasiljevic, 1997: Recent experimentation on 4D-var and first results from a simplified Kalman filter. ECMWF Tech. Memo. No. 240. Reading, U.K., 42 pages.

Rabier, F., A. McNally, E. Andersson, P. Courtier, P. Undén, J. Eyre, A. Hollingsworth and F. Bouttier, 1998: The ECMWF implementation of three dimensional variational assimilation (3D-Var). Part II: structure functions. *Quart. J.R. Meteor. Soc.*, **124**, 1809-1830.

Thépaut, J.-N., P. Courtier, G. Belaud and G. Lemaître, 1995: Dynamical Structure functions in 4D-var: a case study. *Proc. of the 2nd International Symp. on Data Assimilation in Meteorology and Oceanography,* Tokyo, 13-17 March 1995, pp. 129-134.